Numerical Investigation of Eddy Current Losses in Airgap PCB Windings of Slotless BLDC Motors

Guillaume François[1], François Baudart[1], François Henrotte[2], Bruno Dehez[1]

[1]*Mechatronic, Electrical Energy, and Dynamic sytems (MEED)*; [2]*Applied mechanics and mathematics (MEMA)*

Institute of Mechanics, Materials and Civil Engineering (IMMC)

Université catholique de Louvain (UCL)

Louvain-la-Neuve, Belgium

g.francois@uclouvain.be, francois.henrotte@uclouvain.be, bruno.dehez@uclouvain.be

***Abstract*—Replacing classical wire windings with windings printed on flexible circuit boards is a way to improve the performances of slotless BLDC motors. However, these printed windings bring about new design limitations, as they are more subject to eddy current losses than conventional wire windings. This paper aims at evaluating these losses. It proposes a numerical approach to investigate the influence of geometrical parameters like height, width and skewing of the printed copper tracks. The impact of the operating speed is also analyzed, and a heuristic formula to estimate eddy current losses in the case of *zigzag* and *rhombic* winding shapes is finally proposed.**

***Index Terms*—Eddy currents, thin plates, finite elements, PCB winding, Fourier, A-v formulation, 3D modeling, rhombic, zigzag**

I. Introduction

Over the last decades, the use of printed circuit boards (PCB) in electromagnetic components instead of conventional wired windings has grown steadily. This technology helps to drastically decrease the thickness of components in transformers or inductances, leading to more compact designs. It also offers higher precision and reliability during the production process, ensuring more repeatable characteristics of these components. In slotless BLDC machines, it opens the way to new winding geometries and topologies that result in more powerful and efficient motors [1].

However, printed windings have so far demonstrated their superiority over classical windings only at low speed. Indeed, for the same cross section area, printed circuits have wider conductive tracks than classical wires (printed conductive tracks are wide and thin). Therefore, larger areas of conducting material are exposed to a perpendicular time varying magnetic flux, which favors the apparition of eddy currents. At high speed, the Joule losses associated with these eddy currents can deteriorate the performances reached by PCB windings at low to medium speed. It is thus essential to take them accurately into account in the design of high speed motors with such windings. Furthermore, for optimization purposes, it is required to have a quick and efficient evaluation method.

G. François is a FRIA Grant Holder of the "Fonds de la Recherche Scientifique"-FNRS, Belgium.

The aim of this paper is therefore firstly to propose a modeling approach for eddy currents in printed conductive tracks of slotless BLDC motors and, secondly, based on this model, to derive a heuristic formula for eddy current losses.

Since eddy currents in PCB tracks is a 3D phenomenon, which can be hard and time-consuming to solve, section II proposes a two-step approach, based on finite element (FE) simulations, that considerably reduces the complexity of the problem. The approach is then used in section III in a numerical study to establish a heuristic formula relating eddy current losses with height, width and skew of the conductive tracks. Finally, section IV is a comparison of the most traditional motor windings which are the *zigzag* [3] and *rhombic* [2] shapes.

II. Model

A. Problem description and simplifying assumptions

The case of interest is a slotless BLDC motor, Fig. 1 (left). We shall note ω the angular speed of the rotor, p the number of pole pairs and τ the rotor pole pitch. The motor has an active axial dimension h, which also corresponds to the active length of the stator winding. The width of the conductors, measured along the azimuthal direction, is noted λ.

The modeling is done under the following simplifying assumptions:

1) The curvature is neglected, allowing it to transform the cylindrical problem into a planar one (see Fig. 1);

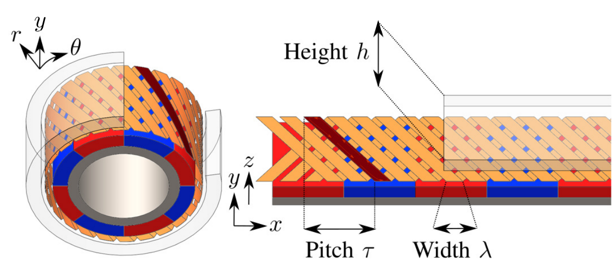

Fig. 1. The radial flux motor with a *zigzag* winding (left) is being unrolled to obtain a planar problem description defined in cartesian coordinates (right) using the transformation $\{r, \theta, y\} \rightarrow \{p\tau\theta/\pi, y, r\}$

2) The axial component of the permanent magnet (PM) field is neglected;
3) Induced currents are assumed to be constant over the thickness g of the track, and to have only in-plane components;
4) The inductive coupling of the tracks is assumed very low compared to the effect of the PM magnetic field. This assumption is discussed in section II-F.

In addition, our study is limited to the fundamental harmonic of the PM magnetic field, which is actually right for a one pole pair rotor with parallel magnetization.

B. Two steps approach

A major difficulty is the multi-scale dimensions of the problem. In classical fractional horse power range motors, the rotor pitch is a few centimeters, whereas the track width hardly reaches the millimeter, and the track thickness is a fraction of a millimeter. From a numerical point of view, this implies that a space discretization that is sufficient for resolving eddy currents in conductors with such aspect ratios will be detrimental in terms of computation time. Various multi-scale approaches have been proposed to deal with this difficulty [4], but these methods apply generally only for problems with symmetries or regular patterns. As we are aiming at establishing a quick approximative estimation of eddy current losses, we decided to split the problem in two successive steps:

- The first step consists in solving a 2D magnetostatic problem in the xy plane in order to obtain the magnetic induction field distribution $\vec{B}_0$ generated by the permanent magnets in the absence of stator conductors.
- The second step consists then in solving the 3D magnetodynamic problem of the conductive track and its nearby environment only, applying the PM field $\vec{B}_0$ moving at a speed $c = p\omega\tau/\pi$ along the x axis as a source term.

C. 2D Magnetostatic formulation

Since slotless motors are considered in this study, the stator-rotor configuration is invariant in the θ coordinate in the absence of conductors. The PM field $\vec{B}_0$ can thus be computed through a simple magnetostatic problem:

$$\vec{\nabla} \times \vec{H}_0 = 0 \text{ on } \Omega \quad (1)$$
$$\vec{\nabla} \cdot \vec{B}_0 = 0 \text{ on } \Omega \quad (2)$$
$$\vec{B}_0 = \mu \vec{H}_0 \text{ on } \Omega/\Omega_M \quad (3)$$
$$\vec{B}_0 = \mu_0(\vec{H}_0 + \vec{M}) \text{ on } \Omega_M \quad (4)$$

where Ω represents the whole domain, Ω_M are the PM domains, $\vec{H}_0$, μ, μ_0 and $\vec{M}$ are respectively the magnetic excitation field, the magnetic permeability, the magnetic permeability in void (i.e. equal to $4\pi * 10^{-7}$ H/m) and the magnetization field of the PM. Gauss law (2) allows defining a magnetic vector potential field $\vec{A}_0$ such that $\vec{B}_0 = \vec{\nabla} \times \vec{A}_0$, which leads to the formulation of the problem:

$$\vec{\nabla} \times (\mu^{-1}\vec{\nabla} \times \vec{A}_0) = 0 \text{ on } \Omega/\Omega_M \quad (5)$$
$$\vec{\nabla} \times (\mu_0^{-1}\vec{\nabla} \times \vec{A}_0) = -\mu_0\vec{\nabla} \times \vec{M} \text{ on } \Omega_M \quad (6)$$

As only eddy currents in the xy plane are considered, the sought B_{z0} field has only a z-component which, due to the second simplifying assumption, does not depend on the coordinate y. Moreover, due to the third assumption, the magnetic field can be evaluated at a fixed position z = ζ corresponding to the mid-plane of the tracks, as illustrated in Fig. 2. Finally, the z-component of the PM field being periodic with a period 2τ, it can be expanded into a Fourier series:

$$B_{z0}(x) = \sum_{n=-\infty,odd}^{+\infty} c_n e^{\frac{j2\pi nx}{2\tau}} \quad (7)$$

where the c_n are the discrete Fourier coefficients. Accounting for the rotation at angular speed ω of the rotor, one has

$$B_{z0}(x,t) = B_{z0}(x - ct) = \sum_{n=-\infty,odd}^{+\infty} c_n e^{jn\left(\frac{\pi x}{\tau} - p\omega t\right)} \quad (8)$$

for the spatio-temporal distribution of the PM field, of which only the fundamental component

$$B_{z0}(x,t) = \hat{B}_{z0} \cos\left(\frac{\pi x}{\tau} - p\omega t\right) \quad (9)$$

is considered in this paper.

D. 3D Magnetodynamic formulation

In the quasi-static approximation, Maxwell's equations and constitutive laws are as follows in the conductor domain Ω_C:

$$\vec{\nabla} \times \vec{H} = \vec{J} \quad (10)$$
$$\vec{\nabla} \cdot \vec{B} = 0 \quad (11)$$
$$\vec{B} = \mu_0 \vec{H} \quad (12)$$
$$\vec{\nabla} \times \vec{E} = -\frac{\partial \vec{B}}{\partial t} \quad (13)$$
$$\vec{J} = \sigma \vec{E} \quad (14)$$

where $\vec{H}$, $\vec{B}$, $\vec{E}$, and $\vec{J}$ are respectively, the magnetic field, the magnetic flux density, the electric field and the current density. Because of Gauss's law (11), the magnetic flux density derives from a magnetic vector potential $\vec{A}$, $\vec{B} = \vec{\nabla} \times \vec{A}$, and substituting into Faraday's law (13) yields:

$$\vec{\nabla} \times \left(\vec{E} + \frac{\partial \vec{A}}{\partial t}\right) = 0 \Rightarrow \vec{E} = -\frac{\partial \vec{A}}{\partial t} - \vec{\nabla}\phi \quad (15)$$

with ϕ the electric scalar potential.

Finally, using (12), (14) and (10), we obtain the classical $A - \phi$ magnetodynamic formulation:

$$\vec{\nabla} \times \left(\mu_0^{-1}\vec{\nabla} \times \vec{A}\right) = -\sigma \frac{\partial \vec{A}}{\partial t} - \sigma \vec{\nabla}\phi \quad (16)$$

The conservation of charge, on the other hand, is imposed with the equation $\vec{\nabla}\cdot\vec{J}=0$, which is the divergence of (10). Assuming uniform electric conductivity, one has

$$\sigma\vec{\nabla}\cdot\vec{E}=0\Rightarrow\sigma\frac{\partial(\vec{\nabla}\cdot\vec{A})}{\partial t}+\sigma\vec{\nabla}^2\phi=0 \tag{17}$$

The permanent magnet rotating field is accounted for in the model by decomposition of the unknown field into two components, $\vec{A}_r = \vec{A}_r + \vec{A}_0$, where $\vec{A}_0$ is a source field verifying $\vec{B}_0 = \vec{\nabla}\times\vec{A}_0$ with $\vec{B}_0$ the PM field computed during the first step, and $\vec{A}_r$ is the reaction field due to the eddy currents induced in stator conductors. Substitution into (16)-(17) and recalling (5) then gives in time domain:

$$\vec{\nabla}\times\left(\mu_0^{-1}\vec{\nabla}\times\vec{A}_r\right)=-\sigma\frac{\partial\vec{A}_r}{\partial t}-\sigma\frac{\partial\vec{A}_0}{\partial t}-\sigma\vec{\nabla}\phi \tag{18}$$

$$\frac{\partial(\vec{\nabla}\cdot\vec{A}_r)}{\partial t}+\frac{\partial(\vec{\nabla}\cdot\vec{A}_0)}{\partial t}+\vec{\nabla}^2\phi=0 \tag{19}$$

or in the frequency domain

$$\vec{\nabla}\times\left(\mu_0^{-1}\vec{\nabla}\times\vec{A}_r^n\right)=-jnp\omega\sigma(\vec{A}_r^n+\vec{A}_0^n)-\sigma\vec{\nabla}\phi^n \tag{20}$$

$$jnp\omega\vec{\nabla}\cdot\vec{A}_r^n+jnp\omega\vec{\nabla}\cdot\vec{A}_0^n+\vec{\nabla}^2\phi^n=0 \tag{21}$$

where $(\cdot)^n$ denotes the n^{th} harmonic complex phasor of the field $(\cdot)$. The source term $\vec{A}_0$ being given as a Fourier series in our case, we solved the frequency domain formulation for the fundamental harmonic only with

$$\vec{A}_0^1=-y\hat{B}_{z0}e^{j\left(\frac{\pi x}{\tau}\right)}\hat{e}_x \tag{22}$$

Finally, after solving (20)-(21), the potentials $\vec{A}^n$, ϕ^n are expressed in time domain, and the eddy currents $\vec{J}$ and the associated Joule losses P are successively obtained through:

$$\vec{J} = -\sigma\frac{\partial\vec{A}_r}{\partial t}-\sigma\frac{\partial\vec{A}_0}{\partial t}-\sigma\vec{\nabla}\phi \tag{23}$$

$$P = \int_{\Omega_C}\sigma^{-1}||\vec{J}||^2 \tag{24}$$

The latter can be solved using first order finite elements. In this study, we have used the Onelab package [6] for interfacing the mesh generator Gmsh [7] and the multiphysics finite element solver GetDP [8]. All three packages are open-source.

E. Reduction of the problem

The two steps approach makes sense only if the magnetodynamic formulation can be solved on a reduced domain. To that end, we firstly investigate eddy current losses in a single track submitted to a magnetic field of amplitude $\hat{B}_{z0}=1$ T at different positions ζ in the airgap (see Fig. 2). The domain of analysis Ω considered here covers the airgap and the magnets. Iron parts are left out of the model and are modeled by setting to zero the tangential component of the magnetic field on the iron-air interfaces, which is a Neuman boundary condition on $\vec{A}$ resulting from the assumption of an infinite magnetic relative permeability for iron. Numerical results for a track height $h=1.5$ cm, width $\lambda=1$ mm, thickness $g=60$ μm, a pole pitch $\tau=1.5$ cm and a speed of

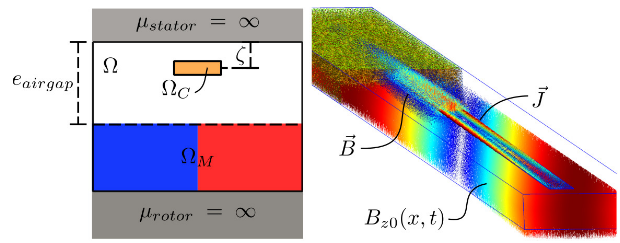

Fig. 2. Domain decomposition from a 2D point of view (left) and example of a finite element simulation of the magnetodynamic part (right)

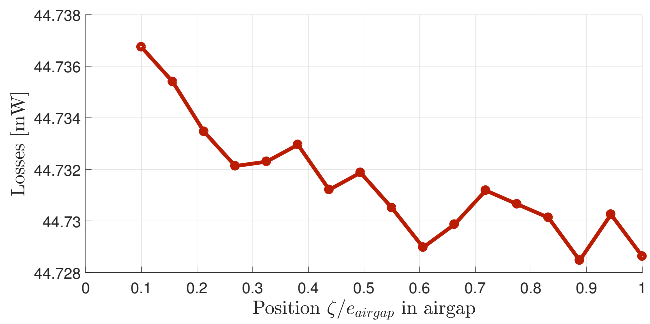

Fig. 3. Variation of the track position in the airgap

60000 rpm are shown in Fig. 3. No impact of the position ζ on the eddy current losses is observed. This can be explained by the fact that the reaction field is much weaker than the PM field $\vec{B}_0$, which also backs up the fourth simplifying assumption of section II-A.

Fig. 4 shows the relationship between the computed Joule losses and the size of the air box, using the same conductive track as previously. Based on these results, a distance d of one millimeter has been considered as a good compromise between the precision on losses and the number of finite elements in the model. Comparison of Fig. 3 with Fig. 4 indicates that the computed losses are close enough, which validates the air box approach.

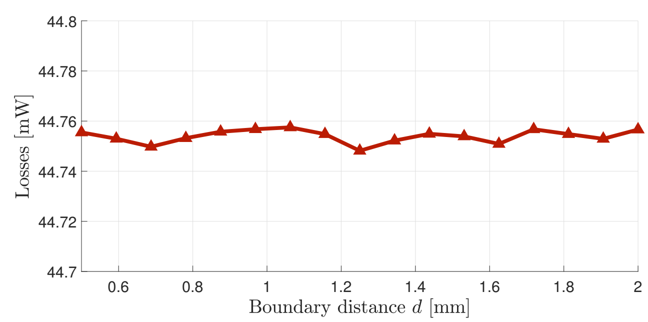

Fig. 4. Evolution of the losses in the track according to the distance of the Dirichlet boundary condition

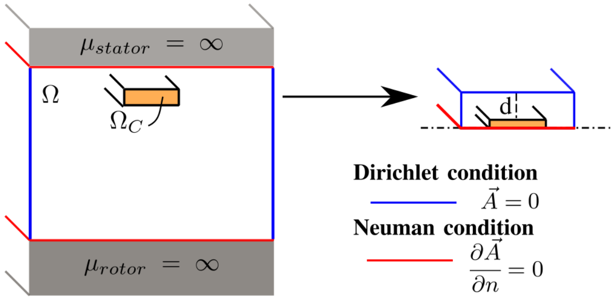

Fig. 5. Reduction of the problem complexity

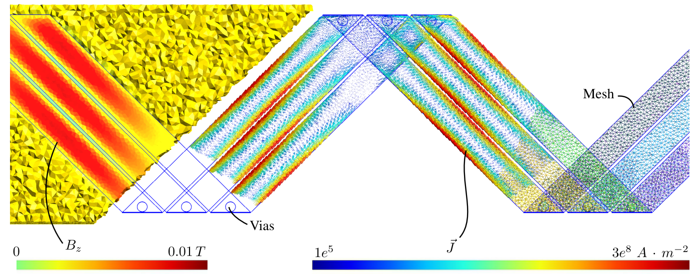

Fig. 6. Multiple conductors connected through vias. From left to right: The z component of the magnetic reaction field; The current density; The mesh.

Finally, without the iron parts, the problem has a plane of symmetry, and only one half of the domain needs to be considered imposing the magnetic field to be normal to the symmetry plane (see Fig. 5).

F. Single track hypothesis

In order to verify the fourth assumption of section II-A, we simulated three conductors disposed parallel to each other, and spanning multiple pole pitches as shown in Fig. 6. We considered the case with $\tau = 1$ cm, $h = 1$ cm, $\lambda = 2$ mm and $\omega = 60000$ rpm. Losses in one track segment are 0.230 W when in isolation (with no effect on it of neighboring track segments), 0.232 W when simulated together with the neighboring segments but non-connected, and finally 0.233 W when taken as part of the full winding. Furthermore, it can be observed in Fig. 6 that the reaction field, not only is weak compared to the source field, but is also concentrated inside the conductors and does not affect significantly neighboring segments.

III. Parametric Analysis

This section develops the methodology we used to establish a heuristic formula for eddy current losses out of numerical simulations. Basically, the physical problem depends on 9 parameters depending on 4 independent fundamental units $(\mathrm{m}, \mathrm{kg}, \mathrm{s}, \mathrm{A})$. A function f_1 thus exists relating those 9 parameters

$$f_1(P_v, \hat{B}_{z0}, \tau, \lambda, h, \omega, \sigma, \mu, g) = 0 \tag{25}$$

where $P_v = P/(g\lambda h)$ is the eddy current losses density in the conductor. The Vaschy-Buckingham theorem or Π theorem [9] states that the same problem can be described by an equivalent function

$$\pi_1 = f_2(\pi_2, \pi_3, \pi_4, \pi_5) \tag{26}$$

involving only 5 dimensionless variables, Table I.

TABLE I
Dimensionless variables of the problem

π_1	π_2	π_3	π_4	π_5
$\frac{\mu P_v}{\omega \hat{B}_{z0}^2}$	$\sigma\mu\omega g^2$	$\frac{\tau}{g}$	$\frac{h}{\tau}$	$\frac{\lambda}{\tau}$

Our problem thus takes the following form:

$$P_v = \mu^{-1}\hat{B}_{z0}^2\omega \quad f_2\big(\sigma\mu\omega g^2, \frac{\tau}{g}, \frac{h}{\tau}, \frac{\lambda}{\tau}\big) \tag{27}$$

A number of observations can be made at this stage:

- Losses are quadratic in the magnetic field. As our magnetodynamic formulation is linear, the current density is expected to be proportional to the source term $\hat{B}_{z0}$, and hence the losses proportional to the square of it.
- Since the source field is directly imposed and the magnetic properties of the environment being considered only at the first step of the approach, we can expect that μ does not appear in the final equation.
- Equations (23)-(24) imply that P_v is linear in the conductivity σ.
- The third simplifying assumption of section II-A makes the problem linear in the track thickness g. The eddy current losses density should therefore not depend on the latter.

A. Variables separation

The next step in the reasoning is to justify that the function f_2 is variable separable. Indeed, if a function of two variables is the product of two functions of one variable, $F(x, y) = X(x) * Y(y)$, then the quotient $F(x, y = y_i)/F(x = x_0, y = y_i)$ will be independent of y_i if the variables x and y are separable, which we shall note $x \perp y$. The ranges of the considered variables are $\lambda \in [0.5; 3]$ mm, $h \in [0.5; 2]$ cm, $\tau \in [0.5; 3]$ cm and $\omega \in [10000 - 100000]$ rpm. The variables σ, μ and g have been kept constant, and equal to $6.56\,10^7$ S/m, $4\pi\,10^{-7}$ Tm/A and 60 μm, respectively.

Fig. 7 indicates that $\lambda \perp \omega$, $h \perp \omega$ and $\tau \perp \omega$, showing that the effects on losses of frequency and winding geometry are decoupled. At 100000 rpm, the difference in $\frac{P_v}{P_{v0}}$ between $h = 0.5$ cm and $h = 2$ cm is only 0.14%. The variation between $\tau = 0.5$ cm and $\tau = 3$ cm is also negligible, as it is 0.25%. However, at that speed, the difference between $\lambda = 0.5$ mm and $\lambda = 3$ mm is 5.44% implying that the variable separation is a bit less accurate. Fig. 8, keeping h/τ and λ/τ constant, suggests that $\tau/g \perp (h/\tau, \lambda/\tau)$ despite that for large values of λ/τ the variable separation becomes less accurate.

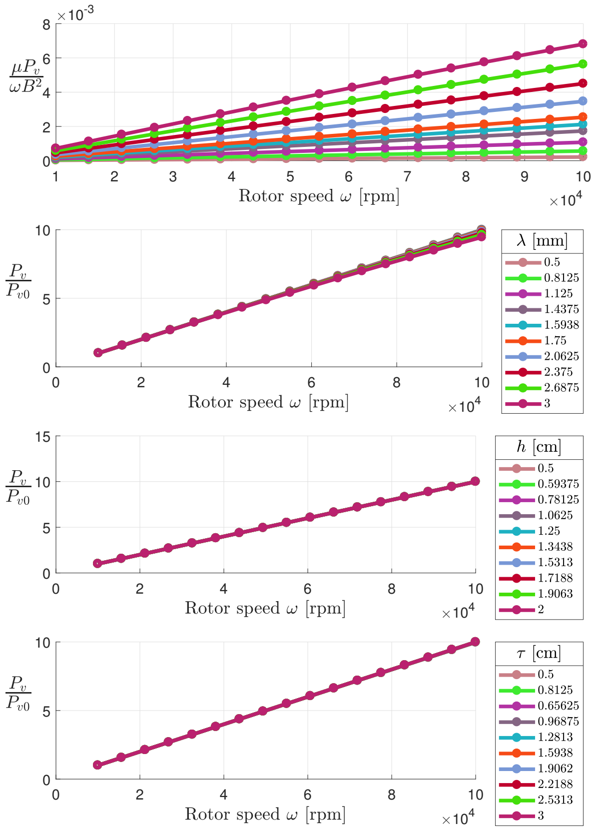

Fig. 7. From top to bottom: Evolution of the variable π_1 for various λ; Evolution of $P_v(\omega)/P_v(10000\text{ rpm})$ for various λ, various h and various τ

Finally, Fig. 9 shows that h/τ and λ/τ can be studied independently. Based on these observations, the eddy current losses density can be written as:

$$P_v = \mu^{-1}\hat{B}_{z0}^2\omega f_4(\sigma\mu\omega g^2) f_5(\frac{\tau}{g}) f_6(\frac{\lambda}{\tau}) f_7(\frac{h}{\tau}) \tag{28}$$

B. Curve fitting

We will assume f_4, f_5 and f_6 can be fitted using monomes. However, this is not the case for f_7. Indeed, as h/τ goes to infinity, the loss density should tend towards a constant value. Therefore, the function f_7, being the only one depending on h, it needs to asymptotically tends towards a constant. This is why it has been chosen as an arctangent function, so that we end up with the following parametric function:

$$P_v = \alpha_0\mu^{-1}\hat{B}_{z0}^2\omega(\sigma\mu\omega g^2)^{\alpha_1}(\frac{\tau}{g})^{\alpha_2}(\frac{\lambda}{\tau})^{\alpha_3}(\tan^{-1}(\alpha_4\frac{h}{\tau}))^{\alpha_5} \tag{29}$$

A learning set of 1582 points uniformly distributed in the space of variables $\{\lambda, h, \tau, \omega\}$ has been used to identify the free α_i parameters. The resulting functions has then been validated on another set of 1159 points. After rounding off the monomial exponents, the following algebraic expression is obtained

$$P_v = 1.218e^{-8}\mu^{-1}\hat{B}_{z0}^2\omega(\sigma\mu\omega g^2)^1(\frac{\tau}{g})^2(\frac{\lambda}{\tau})^2(\tan^{-1}(\frac{\pi}{2}\frac{h}{\tau}))^2 \tag{30}$$

and after simplification of canceling terms, the sought heuristic formula for eddy current losses reads

$$P_v = 1.218e^{-8}\sigma\hat{B}_{z0}^2\omega^2\lambda^2\tan^{-2}\left(\frac{\pi}{2}\tan(\phi)\right) \tag{31}$$

with $\phi = \tan^{-1}(h/\tau)$. This expression is consistent with the observations made above.

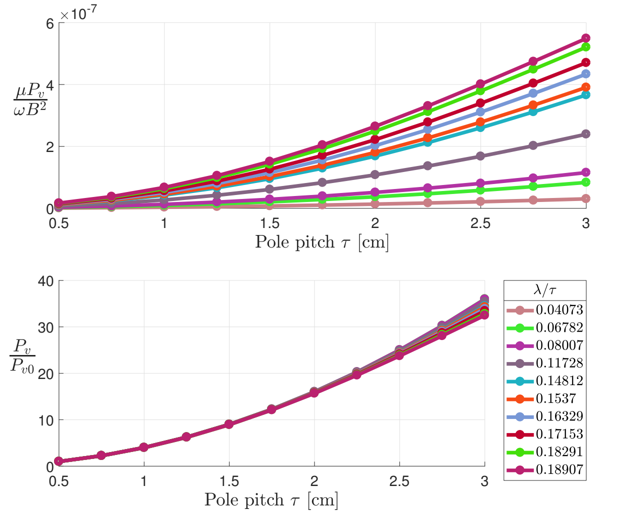

Fig. 8. Evolution of π_1 (on top) and $P_v(\tau)/P_v(0.5\text{ cm})$ (on bottom) with the pitch τ for various sets of $(\lambda/\tau, h/\tau)$

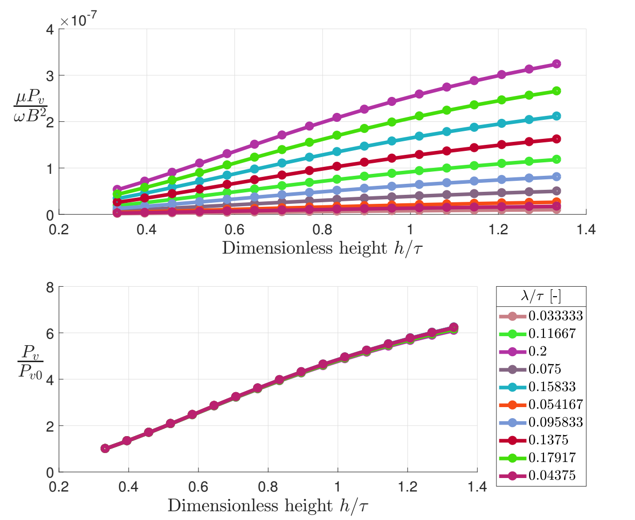

Fig. 9. Evolution of π_1 (on top) and $P_v(h/\tau)/P_v(0.33)$ (on bottom) with h/τ for various λ/τ

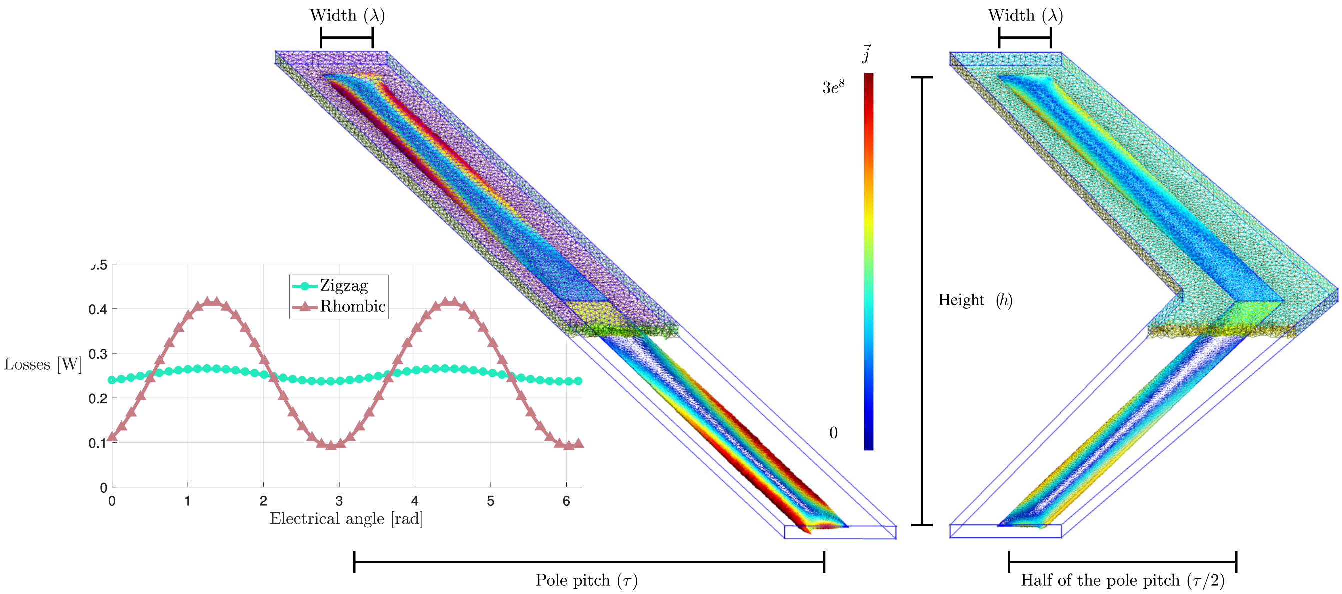

Fig. 10. Current density at 60000 rpm with $\tau = 1.5$ cm, $\lambda = 1.5$ mm and $h = 2$ cm for the *zigzag* (left) and *rhombic* (right) shapes

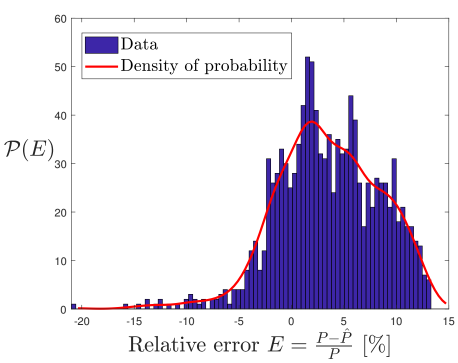

Fig. 11. Distribution of the absolute relative error

The mean of the relative errors μ_E, when compared to the numerical solutions, is 4.84 % and the standard deviation σ_E is of 3.6 %. Fig. 11 shows the distribution of the signed relative error using the fit (31).

IV. Rhombic shape

In the previous section, the conductors were straight segments, spanning over one pole pitch. This configuration corresponds to the classical *zigzag* shape of many slotless motor windings. But another very common configuration is the *rhombic* shape (see Fig. 12). In theory, both configurations are equivalent from the electrical resistance point of view and from the motor constant point of view [10]. In this section, we determine if they are also equivalent from the eddy current losses point of view. To this purpose, the methodology described above has been used, and eddy current losses in the rhombic configuration have been fitted with (29). We obtained the same α_i parameters as for the *zigzag* shape losses, except for α_0 which is by about 4% larger

$$P_v = 1.267e^{-8}\sigma \hat{B}_{z0}^2 \omega^2 \lambda^2 \tan^{-2}\left(\frac{\pi}{2}\tan(\phi)\right) \tag{32}$$

This fit has been obtained on a learning set of 782 points. It has been characterized on a validation set of 1590 points giving a mean of the relative errors μ_E of 3.25%, when compared to the numerical solutions. The standard deviation σ_E is of 2.65 %.

In addition to a slightly higher α_0 coefficient for the *rhombic* shape, we also observe in Fig. 10 that the instantaneous power losses have larger oscillations. Indeed, in the *rhombic* case the conductor is exposed to the magnetic field with twice the volume of its *zigzag* equivalent, but only during half of a pole pitch. However, from a thermal point of view, the rise in temperature would be the same in both cases since the oscillations frequency is by far higher than the thermal time constant of the motor.

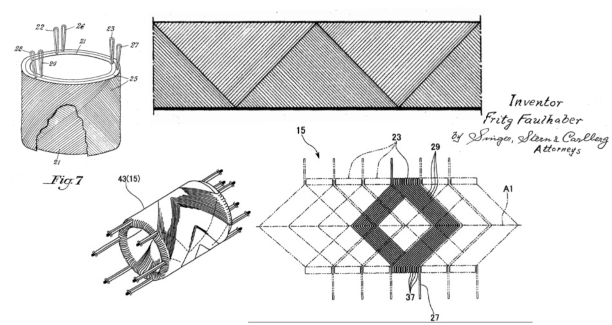

Fig. 12. Drawings of the *zigzag* (top) and *rhombic* (bottom) windings respectively extracted from their patents US3360668 and US6791224

V. CONCLUSION

As a part of a larger program aiming at the efficient design of slotless BLDC motors with printed windings, this paper has proposed a simple and pragmatic approach to model eddy currents losses in PCB armature winding. It has been shown that eddy current losses in the printed tracks can be studied with sufficient accuracy by means of reduced model with one single conductor segment along a pole pitch. This problem reduction allows solving the 3D magnetodynamic equations in a smaller domain, providing still coherent and accurate results. A heuristic formula has then been coined for fast estimation of eddy current losses in case of zigzag and rhombic windings.

To go further and fully validate the fourth hypothesis of section II-A, we should investigate the case of superimposed tracks. Indeed, each layer of PCB winding screens off the next one, reducing the effective magnetic field $\hat{B}_{z0}$ crossing the conductors. Another prospect would be to evaluate the influence of higher harmonics in order to better consider motors with any number of pole pairs and with different kinds of PM magnetizations. At last, we should compare the results of this work to experimental data in order to properly validate our models.

REFERENCES

[1] B. Dehez, F. Baudart and Y. Perriard, ”Analysis of a new topology of flexible PCB winding for slotless BLDC machines”, 2017 IEEE International Electric Machines and Drives Conference (IEMDC), Miami, FL, 2017, pp. 1-8.

[2] R. Rohrer and al., ”Electric motor with multilayered rhombic single coils made of wire”, US patent 2007/0103025

[3] F. Faulhaber, ”Armature winding for rotary electrical machines”, US patent 3360668

[4] K. Hollaus and J. Schöberl, ”Some 2-D Multiscale Finite-Element Formulations for the Eddy Current Problem in Iron Laminates,” in IEEE Transactions on Magnetics, vol. 54, no. 4, pp. 1-16, April 2018.

[5] E. J. Silva and R. C. Mesquita. ”Three dimensional magnetostatics using the magnetic vector potential with nodal and edge finite elements”. in Applied Computational Electromagnetics Society, 1997.

[6] ONELAB. 2018. URL: http://onelab.info/wiki/ONELAB.

[7] C. Geuzaine and J.-F. Remacle, ”Gmsh: a three-dimensional finite element mesh generator with built-in pre- and post-processing facilities”. in International Journal for Numerical Methods in Engineering 79(11), pp. 1309-1331, 2009.

[8] P. Dular, C. Geuzaine, F. Henrotte and W. Legros, ”A general environment for the treatment of discrete problems and its application to the finite element method”. in IEEE Transactions on Magnetics, vol. 34, no. 5, pp. 3395-3398, Sept. 1998.

[9] E. Buckingham, ”On Physically Similar Systems: Illustrations of the Use of Dimensional Equations”, in Phys. Rev. 4, No. 4, 345, 1914.

[10] B. Dehez, M. Markovic and Y. Perriard, ”Analysis of BLDC motor with zigzag and rhombic winding,” The XIX International Conference on Electrical Machines - ICEM 2010, Rome, 2010, pp. 1-5.